An Advanced Level Set Approach to Grain Growth - Accounting for Grain Boundary Anisotropy and Finite Triple Junction Mobility

C. Mießen[a], M. Liesenjohann[a], L.A. Barrales-Mora[a], L.S. Shvindlerman[a], G. Gottstein[a]

[a]*Institute of Physical Metallurgy and Metal Physics, RWTH Aachen University, 52056 Aachen, Germany*

Abstract

The novelty of the proposed level-set approach to grain growth resides in the explicit consideration of structural interfacial elements of the microstructure. The extensions allow to consider anisotropic grain boundary energies and triple junction drag in polycrystalline materials. The simulated predictions were compared to analytical expressions for the growth rate of grains under the influence of a finite triple junction mobility with excellent agreement.

Keywords: grain growth, level set, triple junction mobility, grain boundary energy

Email address: miessen@imm.rwth-aachen.de (C. Mießen)

Introduction

Subsequent to recrystallization, polycrystals undergo grain growth during annealing. Grain growth is driven by the elimination of grain boundary surface to minimize the free energy of the polycrystal. It proceeds by the motion of the grain boundaries (GB) towards their center of curvature an induces a continuous topological rearrangement. This process is decisive for the properties of the resulting microstructure after heat treatment and consequently for the macroscopic properties of crystalline materials.

In an ideal isotropic system, where grain boundary motion is only affected by the local curvature, GB migration leads to a minimization of the total GB in the polycrystal. This evolution is often described as a motion by mean curvature of the GBs [1–7]. In an anisotropic scenario, the evolution of the GB network obeys to different rules of energy dissipation. Dihedral angles at triple junctions depart now from 120° due to different energy densities of adjacent GBs. Additionally, grain boundary motion can also be affected by their possibly distinct mobilities [8–10]. This interplay is reflected in the way microstructure evolution proceeds concomitantly with a change in the misorientation distribution function (MODF) [7]. Furthermore, as shown recently in several investigations [8, 11–14], the properties of triple junctions (TJ) can decisively influence microstructure evolution especially in ultra-fine grained or nanocrystalline materials and lead normally to different grain growth kinetics [15, 16].

Due to the restrictions and difficulties to study experimentally dynamic processes in nanocrystalline materials, a considerable number of investigations [13, 17–23] have been carried out by means of computer simulations. For this task, several models have been developed. They can be roughly separated into two classes based on their deterministic or probabilistic approach to represent microstructure evolution. Vertex models (VM) [13, 17, 20, 24–27], phase field models (PFM) [28–31] and level-set models (LSM) [4, 5, 7] are examples of deterministic algorithms, whereas in the class of probabilistic approaches the Monte Carlo Potts models (MCP) [18, 19, 32] are widely used.

It is also possible to classify deterministic models in the way a microstructure is internally represented. For instance, in vertex or network models only the GBs and their junctions are discretized but not the interior of the grains. In these models, a grain is defined by the volume enclosed by the grain boundaries. In contrast, phase field and level-set methods discretize the volume of the polycrystal and thus, they do only represent microstructural elements such as grain boundaries, triple lines and quadruple junctions implicitly. The abstraction of the microstructure in network models, such as VMs, allows a clear interpretation of the physics of grain growth however at the cost of high computational complexity due to the necessity of implementing rules for topological transformations. On the other hand, in most models where a volume discretization is utilized, the topological transformations are solved automatically by a natural constraint prohibiting overlaps and free space. In these models, however, the topological features are not resolved explicitly and thus effects stemming from structural elements other than the GBs need to be modeled in

roundabout ways. We propose an algorithmic solution to fill this apparent gap in existing grain growth models and demonstrate the consideration of finite, in particular low mobilities of TJ in a 2D level-set framework.

A level-set model for grain growth was introduced by Elsey, Esedoglu Smereka in [7]. They factorized the motion by mean curvature by varying the convolution kernel along the GBs. The challenge of utilizing level-set functions to represent the microstructural evolution of a polycrystal is due to the simultaneous tracking of the isosurface and the affecting scalar field, describing the anisotropy of the GBs on each grid point in an area around the interface. In contrast to VMs, the GB is not an explicit object in PFM or LSM models. The representative implicit function always needs to inherit the structural property of the original GB at each grid point. For this reason, VMs were already successfully extended [13, 17] to consider the effect of finite TJ mobilities in 2D and quadruple junction mobilities in 3D.

Regarding level-set methods, the model developed by Elsey et al. [5, 7] shows great potential due to its computational efficiency and long term stability in 3D. For this reason, in the present contribution, this model was further developed to consider the effect of grain boundary junctions.

The current algorithm was designed for parallel computer architectures by dividing the microstructure into its smallest possible object, i.e. grains. A grain-object stores the corresponding level-set functions, its position in space, and the local topology. Since most of the operations in the level-set approach are applied at a grain level, it is possible to create independent computational tasks and utilize an OpenMP parallelization approach to reduce considerably the time-to-solution. The parallelization is not further discussed in the present contribution but will be published elsewhere [33]. The grain growth level-set (GraGLeS++)[1] simulation tool is provided as open source code.

In the present contribution, we utilized a parallel algorithm to study the effect of finite triple junction mobilities on 2D grain growth. For this, we first analyze the evolution of a four-sided crystal in a well defined environment and compare it to the predictions of an analytical expression derived in [13]. Results on the behavior of different topological classes of an evolving polycrystalline network are discussed subsequently. Finally, the grain growth kinetics of large-scale simulations will be presented and discussed - with special emphasis on the effect of the transient time and initial microstructure on the kinetic growth exponent.

1. Level-set algorithm

Since this method was introduced by Osher and Sethian [1], it has been successfully applied to a vast number of physical processes that involve interface motion. The level-set method is a mathematical framework to describe surfaces and their evolution with time. The method uses an implicit real-valued function

[1] https://github.com/GraGLeS/GraGLeS2D.git

$(\phi(t,x))$ that is evaluated on a fixed Cartesian grid. The isosurface with level zero or *zero level-set* of the implicit function describes the position of the surface (Γ):

$$\Gamma := \{x \in \Omega \,|\, \phi(0,x) = 0\} \subset \Omega \tag{1}$$

Note, that the zero level-set is a subset of the domain Ω, where the function ϕ was defined on. Instead of computing the motion of the parameterized surface, the idea of the method is to track the evolution of the implicit funtion with time. The position of the surface can be always identified as the zero level-set at time $t > 0$.

In order to couple the motion of different phases, these algorithms utilize a "Predictor-Corrector" procedure, where the motion of individual objects is first locally performed and then globally corrected. Originally, the model was only able to simulate ideal grain growth. Only recently, it was enhanced by Elsey et al. [5] to consider different grain boundary energies.

In this section, we present a new level-set algorithm for the simulation of anisotropic grain growth in polycrystalline materials, considering the effect of finite triple junction mobilities in two dimensions.

1.1. Level-set framework - the evolution of individual surfaces

To begin with, we want to link the evolution of a single closed surface to the evolution of a unique level-set function. Therefore, let $\Gamma(0) \subset \Omega \subset \mathbb{R}^2$ be an initial closed surface inside the domain Ω and

$$e[\Gamma] = \int_\Gamma \gamma(n_\Gamma(x))\, dx \tag{2}$$

denote the energy of a surface. $\gamma : \Gamma \to \mathbb{R}$ is a phenomenological function of unit normal vectors, describing the energy density per unit area on the surface. The energy minimization inevitably leads to the evolution of such surface. Thus, any point $x \in \Gamma(t)$ on the surface at a certain time t will move in its normal direction $n_\Gamma(t, x(t))$ with a velocity:

$$v(t, x(t)) = m(n_\Gamma(t, x(t)))\, \gamma\, \kappa(x), \tag{3}$$

where m denotes the mobility of a point $x(t) \in \Gamma$ [34].

Given the initial closed surface Γ_0, we define a function $\phi(t,x)$ on $\mathbb{R}^2 \times \{t \geq 0\}$, which fulfils Eq. (1). Thus, the isosurface with level 0 of the function $\phi(t,x)$ describes the position of the initial closed surface. Such a function is called the level-set function. Since numerous functions meet this requirement an additional constraint is needed to ensure uniqueness of $\phi(t,x)$:

$$|\nabla \phi| = 1,\ \forall x \in \Omega. \tag{4}$$

Thus, the level-set function gives the distance to the nearest point on its zero level set for each $x \in \Omega$. Such function is called a signed-distance function and it will be referred to as d. In terms of the signed-distance

function, we can describe the unit normal by

$$n = \frac{\nabla\phi}{|\nabla\phi|} = \nabla d \tag{5}$$

and the curvature of the isosurface by

$$\kappa = \nabla \cdot n = \nabla \cdot \left(\frac{\nabla\phi}{|\nabla\phi|} \right) = \nabla \cdot (\nabla d)\,. \tag{6}$$

By construction of the total derivative of $\Gamma(t)$ we obtain an equation of motion for the level-set function:

$$\frac{\partial\phi(t, x(t))}{\partial t} - \nabla\phi(t, x(t)) \cdot \frac{\partial x(t)}{\partial t} = 0 \tag{7}$$

$$\Leftrightarrow \frac{\partial\phi(t, x(t))}{\partial t} - \nabla\phi(t, x(t)) \cdot v(x(t))\, n(x(t)) = 0 \tag{8}$$

Utilizing the velocity defined in Eq. (3), we obtain the well-known level-set function:

$$\frac{\partial\phi}{\partial t} - v_n\, |\nabla\phi| = 0. \tag{9}$$

Eq. (9) allows us to track the evolution of an implicit function instead of the original surface. At first hand, this might be perceived as too laborious but the advantages will become clearer in the following.

1.2. Motion by mean curvature

The signed-distance function d represents the position of the initial surface in the domain. We will utilize its properties as expressed in Eqs. (4) to (6), to transform the partial differential equation Eq. (9) to a well-known formulation - the heat equation [4]. This transformation allows us to use an efficient numerical strategy, which utilizes an analytical solution of that equation.

Normalizing the velocity v_n as defined by Eq. (3) in order to depend only on the curvature ($m\gamma(\theta) = 1$) and utilizing the properties from above, Eq. (9) yields

$$\frac{\partial d}{\partial t} - \Delta d = 0. \tag{10}$$

Thus, the motion by mean curvature can be modeled by the heat equation Eq. (10), whose solution is already known and given by

$$G(t, x) = \frac{1}{(4\pi t)^{1/2}}\, e^{-|x|^2/4\pi}. \tag{11}$$

$G(t, x)$ is known as Gaussian kernel. Note, that if $d = g$ on $\mathbb{R}^n \times \{t = 0\}$ far away from the singularity at $(0, 0)$, then the convolution

$$d(t, x) = G(t, x) * g(0, x) \tag{12}$$

provides a solution [35]. The advantage of this approach lies in the reduction of the formal complexity, which describes the effort of solving a problem numerically. The solution strategy given by Eq. (12) requires for a convolution of the initial signed-distance function in space. This represents motion by mean curvature of

the isosurface, as proven above. Without evaluating local curvature at all, one can transfer the convolution step into Fourier space, where the multiple integration in Eq. (12) is simplified into a simple multiplication of Fourier coefficients. This fact is the reason for the success of PSMs and LS algorithms in the past.

1.3. Basic numerical scheme for grain growth

Given an initial microstructure with N-grains, e.g. an EBSD pattern or a Voronoi tessellation [36], we first have to transform the data into a suitable format. For each grain $k \in \{1, \dots, N\}$ we created a surrounding local grid and computed a signed distance function d_k to the ensemble of GBs Γ_k. From now on, the GB is represented by the zero level-set of the corresponding distance function d_k:

$$\Gamma_k = \{x \in \Omega \,|\, d_k(x) = 0\}. \tag{13}$$

By convention the inside is defined to be positive. In the present approach, grains are contained in individual sub-domains (sub-grids) instead of global domains populated by multiple grains (Fig. 1). This approach offers a flexibel data structure that enables a direct parallelization strategy at the grain level. Furthermore, the evolution of individual grains, neighborhoods or topological transformations can be specifically investigated. An additional, non-trivial, benefit is the reduction of the consumed memory. The definition of an unique sub-domain for each grain resulted in considerably less idle memory (Fig. 1).

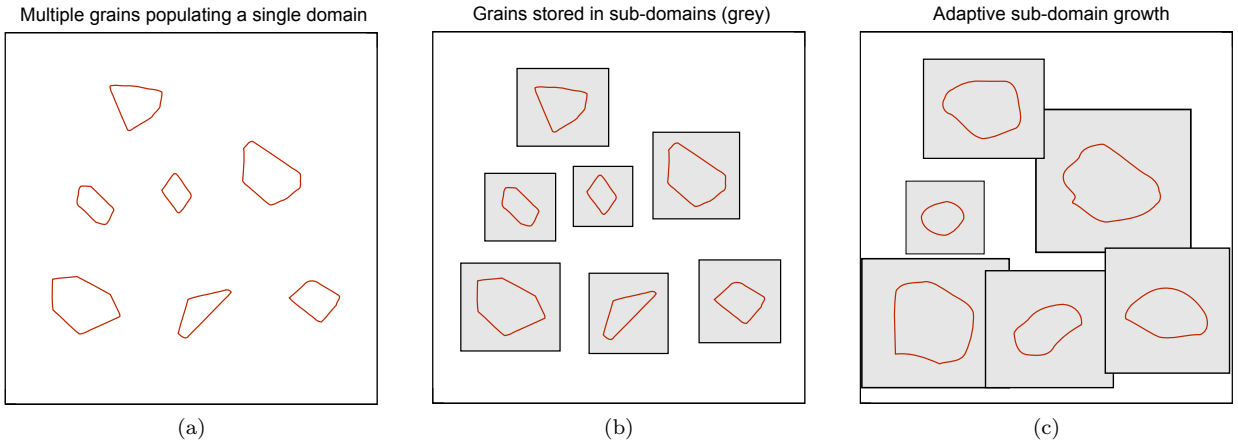

Fig. 1: In the original approach one level-set function is defined in the whole domain containing a set of disjunct grains (a). In (a), memory allocation is needed for all the white space. Memory optimization (b) is achieved by storing grains in individual sub-domains, where only shaded areas required allocation. Additionally, the formal complexity of the algorithm decreases because the overlapping (c) of sub-domains allows for easier identification of the neighborhood of grains.

The basic algorithm for diffusion generated motion using signed distance functions was already described in [4]. A numerical scheme to couple the motion between a finite number of grains is presented in [7] and reproduced here for convenience:

1. Convolution-/Predictor step; compute the motion by mean curvature

$$d_k^p(x, t + \Delta t) \; = \; G_{\Delta t}(x) \; * \; d_k(x, t) \tag{14}$$

2. Comparison-/Corrector step; remove overlaps and free space in the network

$$d_k^c(x, t + \Delta t) \; = \; \frac{1}{2} \left(d_k^p(x, t + \Delta t) \; - \; max_{j \neq k} \, d_j^p(x, t + \Delta t) \right) \tag{15}$$

3. Redistancing-/Reinitialisation step; recompute the signed-distance function to the isosurface

$$d_k^c(x, t + \Delta t) = 0. \tag{16}$$

2. Algorithm extension - detecting and considering structural elements

Whereas the basic scheme presented above can be used to simulate anisotropic grain growth by varying G pointwise in dependency on the GB energy density γ, it is not able to consider the effect of the GB junctions on grain growth [7]. The reason for this lies in the volume discretization of the grains that does not allow for a direct identification of the positions of the GB junctions (triple lines and quadruple junctions) and therefore an association of a property with the volume of such element seems at first sight impossible. In order to consider these features, which are highly relevant for nanocrystalline materials [37, 38], it is necessary to enhance the simulation scheme presented above.

2.1. Anisotropy correction

To begin with, we assume that the velocity field in the neighbourhood of the GB defined on each grid point is known. Furthermore, two LS functions describe the consecutive positions of a GB (double-buffering), before and after the convolution step. The key idea of this numerical scheme is the connection between two metrics, one operating on surfaces and the other on level sets [39]. Comparing both states of the level-set function allows identifying a variation in height at each grid point given by

$$s_t \; := \; \frac{\partial \phi}{\partial t} \; = \; -v_n \left| \nabla \phi \right| , \tag{17}$$

where v_n is the variation of the surface in normal direction. Near the zero level-set the first distance function satisfies $|\nabla \phi| = 1$ whereas the second one approximately does so. This observation simplifies the connection between the two metrics shown in Eq. (17) and Fig. 2.

In the model, it is possible to describe the properties of the grain boundaries at any point. For instance, if the mobility m and the grain boundary energy γ depend on the misorientation or the grain boundary plane, a continuous function containing this information can be defined for the contour of a grain. Initially, this function does not affect the motion of the grain boundaries because it resides in a different space than the

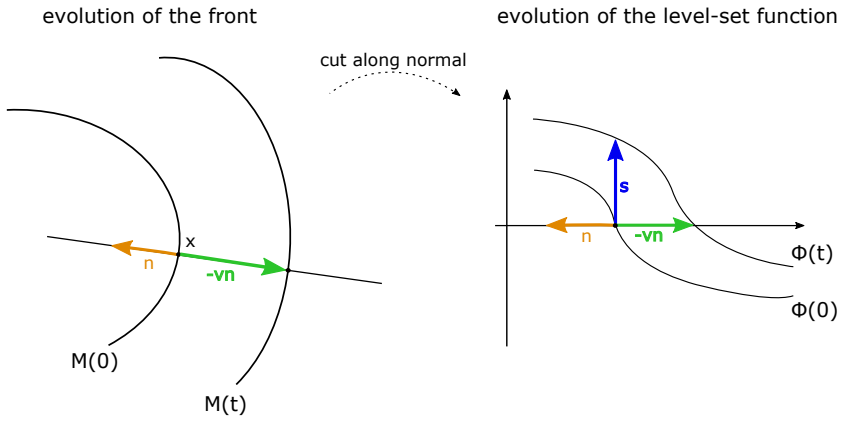

Fig. 2: A metric on surfaces meassuring the distance of interfaces in normal direction (v_n) and one on level-sets meassuring the variation in height (s) of the associated level-set funtions can be connected utilizing the gradient of the level-set function. This connection is the key for identifying and messuring the behaviour of the implicitly represented GB.

grains. In order to consider these dependencies, the function (i.e. the properties) must be first transferred to the signed distance function. This can be done by introducing the following sort of "Euler-forward step" to the algorithm:

1.

$$v_n = \kappa_s \; = \; (d_k^c(x, t - \Delta t) \; - \; d_k^p(x, t + \Delta t))/\Delta t = s_t \tag{18}$$

2.

$$d_k^{p,new}(x, t + \Delta t) = d_k^c(x, t - \Delta t) \; + \; (v_n w \Delta t) \tag{19}$$

where w is a scalar to describe the anisotropic components of the normal velocity. While the slope of the convoluted function remains nearly unchanged near the isosurface, the isosurface moves by a parallel shift of all level-sets into their normal directions [4].

In this case, only the signed distance function exists as an implicit representation, the reverse mapping of grid point to nearest point on the grain boundary is not obvious. To the best of our knowledge, an algorithm to solve the problem point-to-polygon-distance is at least $O(m^2 n)$, where n =number of faces and m = number of grid points per direction of the local grid. To reduce the formal complexity of this problem, we evaluate only in a tube around the isosurface reducing effectively the size of the volume to test. In the following section we suggest a strategy to identify the nearest point on the the GB to a point $x \in \Omega$ at a certain time t utilizing a segmentation of the grain boundary representing areas with different physical properties.

2.1.1. Approximation and positioning of implicit objects

In order to consider the effect of the properties of structural elements, such as GB- and TJ mobilities, we first need to define these quantities along the GB and in a second step to pass them to the signed distance function. The identification of the TJs is crucial for a successful segmentation of an individual GB. We utilize a marching squares algorithm [40] to locate an approximation of the GB itself that is stored as set of linear segments. The algorithm can be extended to identify TJs or quadruple junctions by investigating a second data structure holding the information on the closest neighbor grain for each grid point. Since the corners of the marching square correspond by definition to grid points, the TJs can be identified during the application of the marching squares algorithm simply by comparing the neighboring grains stored in the secondary structure for grid points. Once three different grains are found for a square, we define the TJ to be in the barycenter. Secondly, we project the point onto the isosurface as seen in Fig. 3, represented by a linearization. The maximum error of this positioning routine is bounded by $\sqrt{2}h$, where h denotes the equidistant space between two grid points. Continuing the iteration along the isosurface we can identify the set of triple points $\Xi := \{\xi \in \Gamma\}$ of the current grain.

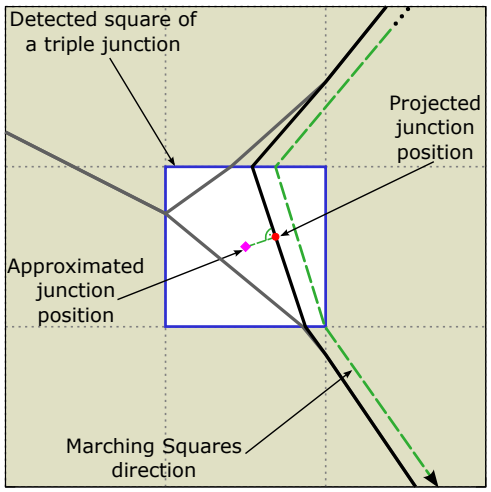

Fig. 3: A modified marching squares algorithm is utilized for the reconstruction of the GB and the positioning of triple junctions. The green dashed line shows the iteration direction of the blue square (marching square) covering four adjacent grid points. A triple junction is identified by detecting three different grains (grey and black solid lines) to be nearest to the four active grid points. The position is first assumed to be in the barycenter of the square and then projected to the the contour line representing the GB. Dotted lines represent the lattice formed by the grid points.

2.1.2. Segmentation of the Grain Boundary

Formally, we define a scalar field $W(x,t) : \Omega_k \to \mathbb{R}^+; (x,t) \mapsto w$ for each sub-domain $\Omega_k \subset \Omega$. Let $d_M(\cdot,\cdot) : M \times M \to \mathbb{R}^+$ be a metric on the manifold $M \subset \Omega_k$. At first the scalar field will be constructed

in such a way that it is continuous on the manifold $M_0(x,t) := \Gamma$. Here, c_1 , $c_2 \in \mathbb{R}^+$ denote two critical distances. The mapping will be defined piecewise along the isosurface and will distinguish three general cases utilizing the set of triple junctions $\xi \in \Xi$:

- Default: Along a GB segment between the grain i and j the weight is set to $w := \gamma(\theta_{i,j})\, m_{i,j}$. A point belongs to such a sector, if

$$min_{t \in T}\, d(t,x) > c_2. \tag{20}$$

- Type 1: In the area around a triple junction $t \in T$, the weight is set to $w := \sigma_i\, m_{ijk}$, where m_{ijk} denotes the mobility of the triple junction ξ_{ijk} separating the grains i, j, and k. A state of equilibrium at a triple junction is defined by:

$$n_{ij}\gamma_{ij} + n_{jk}\gamma_{jk} + n_{ki}\gamma_{ki} = 0, \tag{21}$$

  Utilizing this assumption, the energy densities of the adjacent GBs can be assigned to coefficients σ associated with each grain: $\gamma_{ij} := (\sigma_i + \sigma_j)/2$ as defined in [5]. Thus σ substitudes the GB energy density γ applicable to the level-set function. A point belongs to such a sector, if

$$min_{\xi \in \Xi}\, d(t,x) < c_1. \tag{22}$$

- Type 2: The interpolation sector assimilates the cases described above. A point belongs to such a sector, if

$$min_{\xi \in \Xi}\, d(t,x) \geq c_1 \wedge min_{\xi \in \Xi} d(t,x) \leq c_2. \tag{23}$$

Thus, the scalar field W holds the anisotropy components of the normal velocity at each point of the GB. To derive a rule of motion for the corresponding level-set function, we need to project these quantities onto the surrounding set of grid points. For an arbitrary point x, we define the extension of the mapping:

$$W(x,t) := W(y \in \Gamma(t) \,\|\, min\, \|y - x\|\,, t),\ \forall x \in \Omega \tag{24}$$

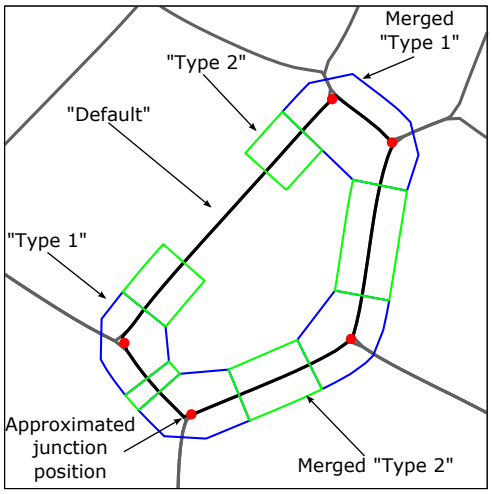

Fig. 4: Grain boundaries and triple junctions are discriminated by the utilization of sectors, where the properties of the structural elements are smoothly applied. Triple junctions and the transition to a grain boundary are represented respectively by type 1 and 2 sectors. Once the length of a grain boundary decreases below a critical distance, two sectors of the same type are automatically merged.

3. Simulations

Combining the basic numerical scheme, see Eqs. (14) to (16) with our extension Eqs. (18) and (19) and utilizing the corresponding anisotropy field Eq. (24) we developed a computational scheme, which enables to identify and distinguish between areas with different physical properties along an isosurface surrounding the interior of a grain. The algorithm is capable of mapping a varying mobility along a certain GB. Furthermore, we are able to recognize topological transformations and record them for statistical investigations.

As already mentioned, an ensemble of GBs surrounding a single grain is represented by a single implicit function. As a consequence, the convolution step moves the entire GB towards its center of curvature, ignoring the presence of TJs and their effect on GB motion. Thus, these properties are firstly neglected to successfully divide the microstructure into single grains and take advantage of an efficient solution strategy. In the comparison step the predicted motion is corrected by the restriction of complete domain covering. In this way, free space and overlaps are removed and junctions are recreated at the residual positions determined by the individually predicted motions of all adjacent grains. This procedure implies an unlimited mobility of the re-created junction.

Our goal was to trigger the implicit function in such a way that a motion was obtained which considers the presence of junctions with finite mobilities. Therefore, we inhibited the motion of the level-set function on a segment around the projection point of the triple junction - see Figs. 3 and 4. In all the simulations, grains were sampled with 20 points on average in any direction. This number was found to be the minimum

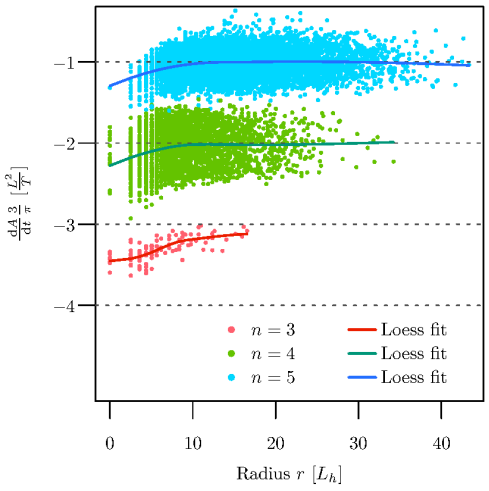

Fig. 5: The area rate of change of the grains with 3,4,5 faces during ideal grain growth of a polycrystal with initially 50000 grains was plotted versus the grain radius. We observed a constant mean shrinkage rate for grains with radius $r > 10 \cdot L_h$, where L_h denotes the distance of two adjacent grid points.

resolution for excellent accuracy as substantiated by the convergence to the solution of the von-Neumann-Mullins equation of the measured data points (Fig. 5). Nevertheless, it is evident that larger deviations are observed systematically for small grains. This is caused by the fact that the curvature cannot be accurately calculated once the grains are resolved by insufficient grid points. This effect is reflected as an acceleration of the shrinkage rate. Obviously, three-sided grains are more affected as they are more prone to possess a significantly smaller than average size Figs. 5 and 6.

Utilizing this resolution, we needed less than 50KB per grain to store all corresponding information. Counting the resulting amount of memory used to store an ensemble of grains defined on a 2D grid with $M \times M$ points in local level-set functions, we found 4 to be an upper bound for the factor of superposition of the original domain. Thus, a network with one million grains consumed less than 50GB RAM. The simulations were performed on BCS machines of the High Performance Computer Cluster (HPC) of the RWTH Aachen University, which owns Intel Xeon X7550 processors with 4×4 sockets and a total of 128 physical threads utilizing 256GB RAM.

3.1. Effect of finite triple junction mobilities

It is now accepted that the mobility of triple junctions [9] can be finite and thus, influence the evolution of a microstructure during grain growth. A triple junction is the point in 2D, where three grain boundaries intersect. In the level-set method, grain boundaries are not perfectly continuous; their resolution depends on the subjacent grid. For this reason, a TJ cannot be considered as a 0-dimensional mathematical object with unique properties. To model the effect of such features, it is necessary to apply special properties to

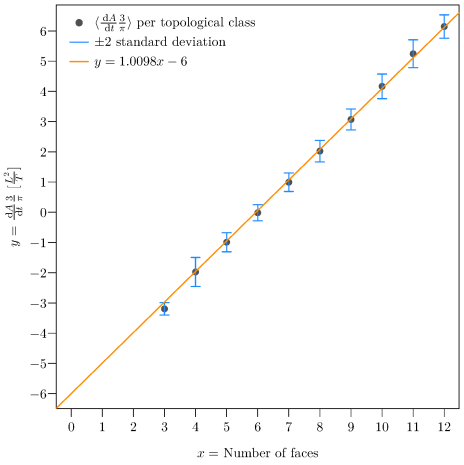

Fig. 6: The average rate of change for topological classes $3 - 12$ shows that the von-Neumann-Mullins relation is predicted accurately by our model. We found a deviation of less than 1% for the area deviation utilizing a discritization of 20 grid points in average. Comparatively, 3% deviation is observed when a resolution of 10 grid points is utilized.

the region close to a triple junction. The size of this region is defined by the resolution of the grid. Inside of this volume, which corresponds to sectors of type 1, the mobility is defined by an effective mobility m_{eff} as:

$$m_{\text{eff}} = \frac{1}{\frac{1}{ds\, m_{\text{TJ}}} + \frac{1}{m_{\text{GB}}}} \tag{25}$$

where ds denotes the length of the sector around the TJ and m_{GB} is the average mobility of the adjacent GBs. The effective mobility and the mobility of a single GB have the same units. To validate our approach, a simple scenario was investigated. A regular four-sided-grain was simulated in a well-defined neighborhood, see Fig. 7. First, the network was relaxed until the four GB segments became curved and started moving inwards. Once this occurred, the mobility of the four "Type 1" sectors was defined to be finite, i.e. $m_{\text{TJ}} \in (0, 1]$, where 1 represented a normalized infinite mobility of the triple junction. As a result, the GBs straightened due to the retardation of the area around the TJ, as evident from Fig. 7.

To quantify the impact of a finite TJ mobility on the evolution of that single grain, we compared the area rate of change $\dot{A}$ to an analytical relationship (referred to subsequently as polygon approach) derived in [13] in dependence on the parameter Λ, which characterized the effect of a finite triple junction mobility:

$$\Lambda = \frac{m_{TJ}\, a}{m_{GB}} = \frac{sin\left(\frac{\pi}{n}\right) - sin\left(\beta - \frac{\pi}{n}\right)}{2\, sin\left(\frac{\beta}{2}\right) - 1} \tag{26}$$

Note that a is defined as the average face length of a grain whereas β denotes the turning angle. The classical von Neumann-Mullins relationship [41] can be expressed as a function of the turning angle, which in turn can be obtained from Eq. (26):

$$\dot{A} = \frac{-m_{GB}\, \gamma}{2} (2\pi - n\beta) \tag{27}$$

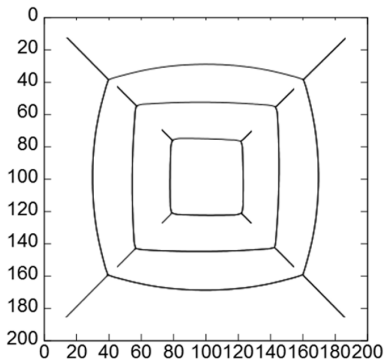

Fig. 7: The effect of a reduced TJ mobility on the shape evolution of a four sided grain is shown. After an isotropic relaxation the GBs became curved and started moving inwards (outermost grain). Once the grain reached this stage, a finite mobility of the triple junctions was applied and the grain boundaries became flat (intermediate and innermost grains).

To cover a wide range of Λ, we required six simulations starting with the same initial configuration sampling different TJ mobilities. For simplification, the GB mobilities were defined to be equal and constant during the whole simulation. The evolution of the area rate of change of the four-sided grain with respect to the parameter Λ was described with excellent accuracy by discretizing the interior with 80 grid point per direction, as seen in Fig. 8.

Next, we investigated the behavior of a polycrystal with $50,000$ grains using only 20 grid points per direction as an average of interior points per grain. We classified grains by their number of faces, in order to determine their affiliation to a particular evolution rule. Fig. 10 reveals the growth and shrinkage rates of the topological classes $3, 4, 5, 7, 9$ and 12. In order to investigate the area evolution depending on different TJ mobilities, we conducted nine simulations to cover a sufficiently large range of the parameter Λ. In agreement with the provided analytical solution, we observed growth rates converging to the predictions of the von-Neumann-Mullins law for large values of Λ. This upper limit is obtained either by grains of large size, hence a large a in Eq. (26) or an effective TJ mobility with values near 1 (indicating an infinite mobility of a TJ). The former was a continuously changing parameter throughout one simulation while the latter was constant and determines the starting point of the Λ values. For small results of Λ we found a tremendously reduced volume change rate in all classes. To determine an empirical average of the growth rates for a certain topological class we used a non-parametric fit averaging all realizations in a certain bin of Λ. Thus, we could compare with the theoretical expectations of the analytical approach of the growth rate depending on Λ. The largest deviation was found for grains with three faces, which were almost always very small grains, see Fig. 10. The main reason was in the insufficient discretization of the smallest grains at least in one direction. A rough discretization affects the convolution step because opposing faces drag each other due to a insufficient number of grid points in the interior of the grain. The evolution of small grains had a crucial impact on the number of topological events and therefore on the characteristic properties of

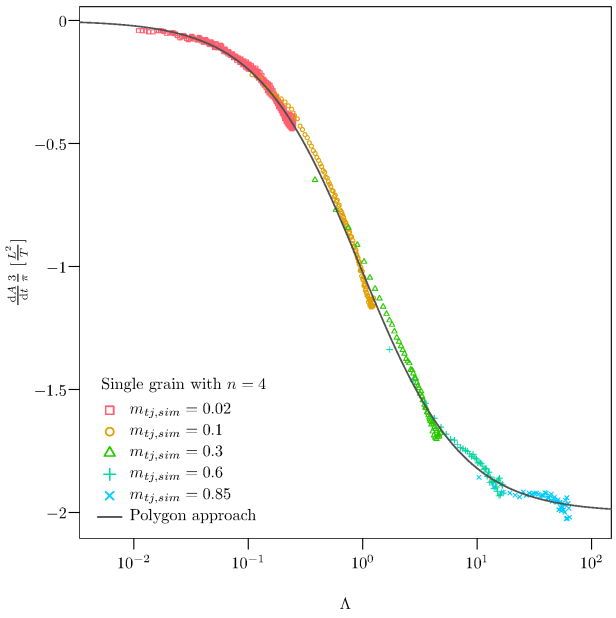

Fig. 8: The parameter Λ (Eq. (26)) characterizes the impact of a reduced TJ mobility on grain growth. For the simulated four-sided grain, the rate of change converged to the von-Neumann-Mullins relationship for $\Lambda \to \infty$. For $\Lambda \to 0$, we observed a reduced area rate of change in agreement with Eqs. (26) and (27). In total five simulations were utilized to cover a sufficient range of the parameter space.

the network changing with time. To understand these repercussions, we compared the equilibrium grain size distribution for different TJ junction mobilities. The finite mobility was equal for all junctions in the polycrystal as before. Fig. 9 was generated with data of five simulations starting from the same initial population sampling different TJ mobilities. This comparison depicts the observation of the magnified life expectancy of small grains. The peak of the distribution was reduced by about 33% for the case of the lowest triple junction mobility compared to ideal grain growth. The missing grains moved apparently to the lower tail of the distributions. Interestingly, the upper tail was strongly affected, too. The five grain size distributions represent the state of the polycrystal after a fixed simulation time, and the resulting mean grain sizes differ due to the reduced energy dissipation near the triple junctions. Thus, the effect of the enlarged upper tail is just an impact of the slowed down kinetics because the average grain area is smaller.

3.2. Growth Kinetics of Networks in the Triple Junctions Regime

A further analysis of the grain growth kinetics showed the effect of a reduced mobility of triple junctions. Fig. 11 clearly indicates that, as the TJ mobility decreases, the grain growth exponent increases from a minimum value of 1.07 to a maximum of 1.41, which is comparable to values found in similar simulations [13, 17, 21] with different starting grain size distributions.

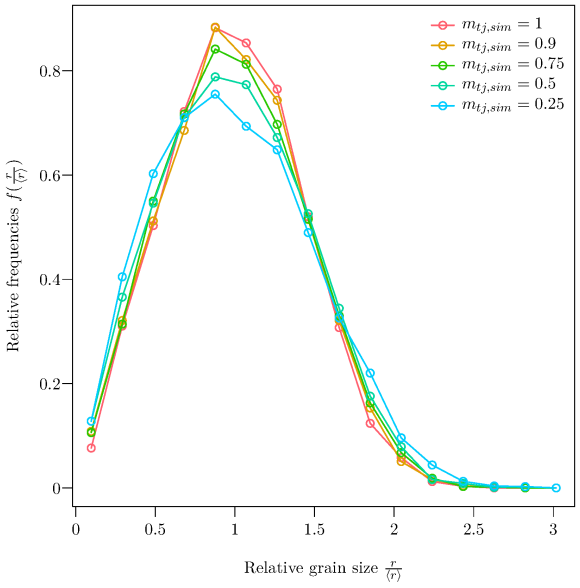

Fig. 9: For quasi-stationary evolving polycrystals with different TJ mobilities a variation in the grain size distribution was observed. By decreasing the mobilty we found a bigger population in the lowest bins, while the peak of the distribution decreased. This effect reflects the increased life expectancy of small grains.

Grain growth kinetics are usually utilized to discriminate between triple junction and grain boundary kinetics. In 2D, grain boundary-controlled grain growth is theoretically characterized by a linear change of the average grain area with time: $A \sim t$. By contrast, a parabolic behavior is expected for TJ controlled grain growth: $A \sim t^2$. Simulations utilizing the Monte Carlo-Potts Model [18] confirmed this expectation. In previous investigations [13, 17], it was contended that only the kinetics might not be enough to determine whether thermal stability was caused by these structural features of the microstructure. This was also substantiated by the present study (Fig. 11).

From a physical point of view, it is obvious from Fig. 10 that the characterization of the evolution of a polycrystal by only the mean grain size is insufficient. Thus, strictly-speaking grain growth in a polycrystal governed by a small triple junction mobility will be in a non-stationary state for an infinite time. Any grain close to collapse will be affected by a reduced energy dissipation caused by the size dependency of the TJ drag.

Nevertheless, from an engineering point of view one can try to extract information on the state of the polycrystal by investigating the skewness of the grain size distribution Fig. 11. This is utilized here to characterize the possible "quasi-stationarity" of the process. Low TJ mobilities cause usually much longer transient times. From Fig. 11, it is possible to conclude that depending on the magnitude of the finite mobility of TJs a quasi-stationary state can be achieved. It is noted, however, that this state can be as well

affected by other physical constraints that influence the equilibrium distribution of a microstructure.

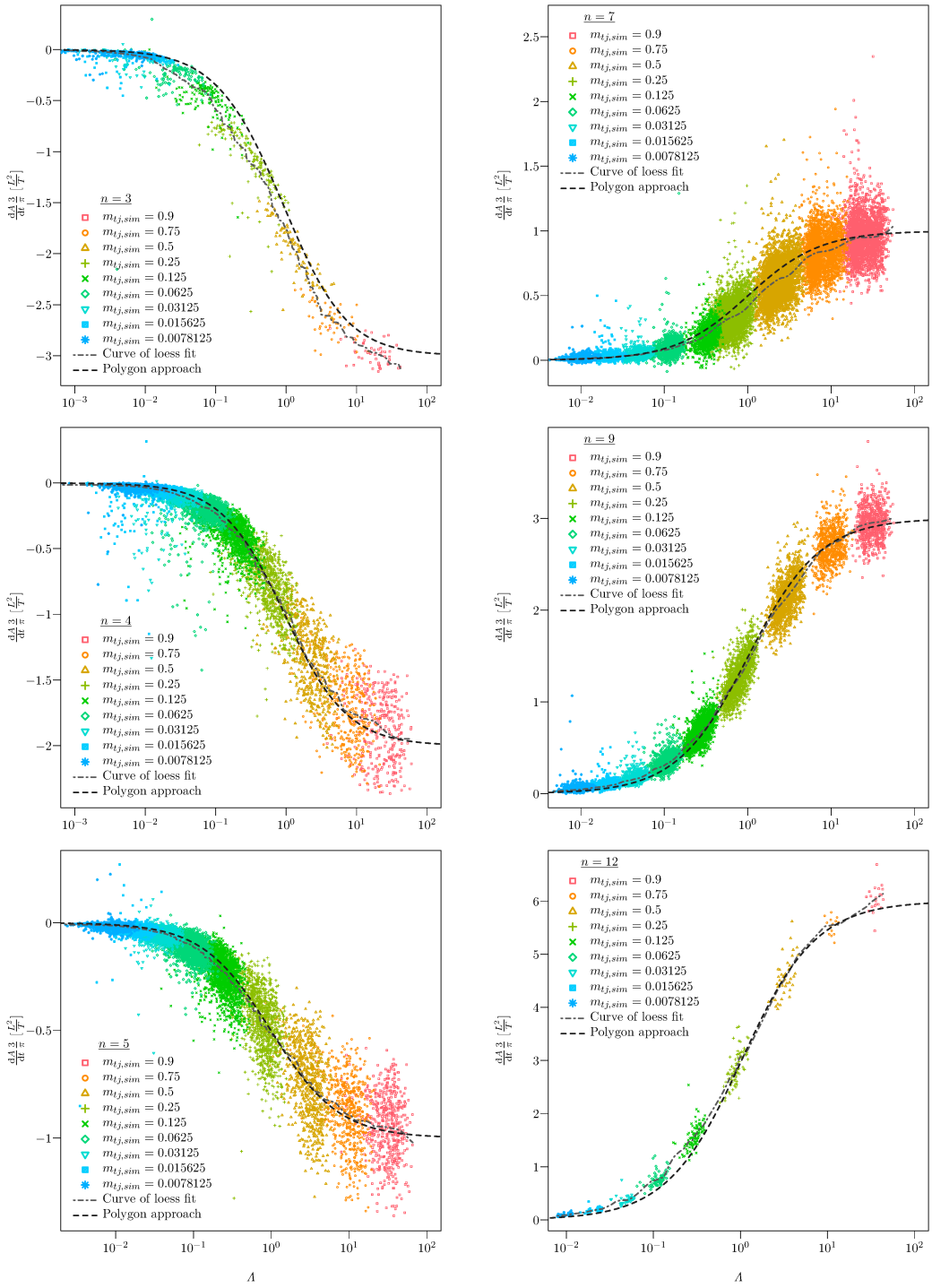

Fig. 10: Grains of a polycrystal with 50.000 grains were clustered by their number of neighbors. The growth rates of these grains with different topological classes were plotted against the parameter Λ that characterizes the effect of triple junctions. As expected, depending on the number of faces a different growth behaviour was observed. The results convergence to the von-Neumann-Mullins relation for all classes with $\Lambda \to \infty$ and a reduced area rate of change for $\Lambda \to 0$.

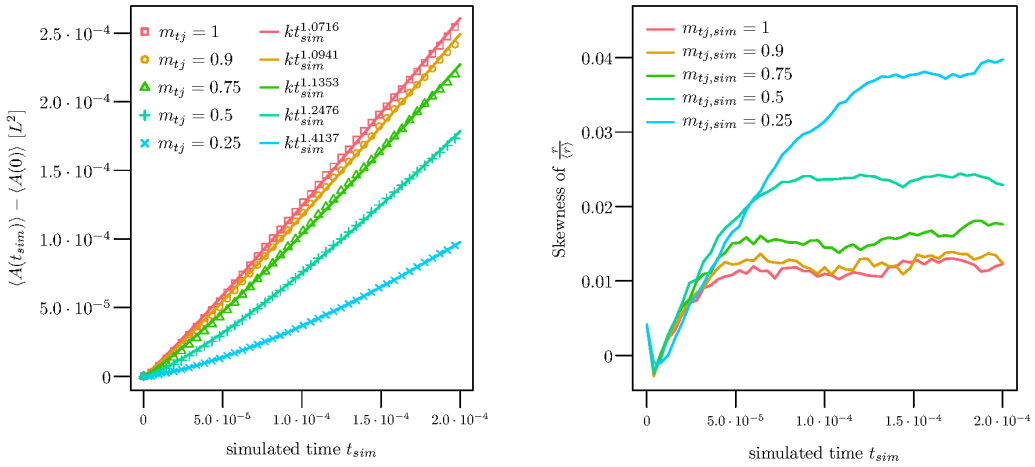

(a) (b)

Fig. 11: The effect of the triple junctions on the kinetics of the polycrystals (a) is expressed by an increase of the growth exponent from the unity. A reduced mobility extended this transient zone.

4. Conclusion and Outlook

The level-set method is computationally superior to other competing approaches to grain growth phenomena by efficiently mapping GB curvature and topological events which guarantees long term stability.

The challenge is the complexity of transferring the properties of structural interfacial elements to the implicit function. In this contribution, we presented a method suited for parallel computational architectures to account for the effect of GB anisotropy and triple junctions on microstructure evolution. The influence of triple junction drag was studied in detail and compared to a theoretical approach with excellent agreement. This extends the range of grain growth scenarios, which the level-set method is capable to manage.

Our future goal is to extend the presented method to 3D grain growth and to consider explicitly quadruple junctions as well. Since the proposed level-set algorithm is highly parallelizable, future investigations on 3D grain growth will profit from recent developments on modern computer architectures.

Acknowledgements

The authors gratefully acknowledge the financial support from the Deutsche Forschungsgemeinschaft (DFG) within the "Reinhart Koselleck-Project" (GO 335/44-1) as well as the FZJülich and the RWTH Aachen University for granting computing time within the frame of the JARAHPC project no 6687.

References

[1] S. Osher, J. A. Sethian, Fronts propagating with curvature-dependent speed: Algorithms based on hamilton-jacobi formulations, Journal of Computational Physics 79 (1) (1988) 12–49.

[2] P. Smereka, Semi-implicit level set methods for curvature and surface diffusion motion, Journal of Scientific Computing 19 (1-3) (2003) 439–456.

[3] S. Esodoglu, P. Smereka, A variational formulation for a level set representation of multiphase flow and area preserving curvature flow, Communications in Mathematical Sciences (2008) 125–148.

[4] S. Esedoglu, S. Ruuth, R. Tsai, Diffusion generated motion using signed distance functions, Journal of Computational Physics 229 (4) (2010) 1017–1042.

[5] M. Elsey, S. Esedoglu, P. Smereka, Diffusion generated motion for grain growth in two and three dimensions, Journal of Computational Physics 228 (21) (2009) 8015–8033.

[6] M. Elsey, S. Esedoglu, P. Smereka, Large-scale simulation of normal grain growth via diffusion-generated motion, Proceedings of the Royal Society of London A: Mathematical, Physical and Engineering Sciences 467 (2126) (2010) 381–401.

[7] M. Elsey, S. Esedoglu, P. Smereka, Simulations of anisotropic grain growth: Efficient algorithms and misorientation distributions, Acta Materialia 61 (6) (2013) 2033–2043.

[8] G. Gottstein, A. H. King, L. S. Shvindlerman, The effect of triple-junction drag on grain growth, Acta Materialia 48 (2) (2000) 397–403.

[9] G. Gottstein, L. S. Shvindlerman, Triple junction drag and grain growth in 2D polycrystals, Acta Materialia 50 (4) (2002) 703–713.

[10] G. Gottstein, Y. Ma, L. S. Shvindlerman, Triple junction motion and grain microstructure evolution, Acta Materialia 53 (5) (2005) 1535–1544.

[11] D. Mattissen, A. Wr, D. A. Molodov, L. S. Shvindlerman, G. Gottstein, In-situ investigation of grain boundary and triple junction kinetics in aluminium 10p.p.m. magnesium, Journal of Microscopy 213 (3) (2004) 257–261.

[12] D. Mattissen, D. A. Molodov, L. S. Shvindlerman, G. Gottstein, Drag effect of triple junctions on grain boundary and grain growth kinetics in aluminium, Acta Materialia 53 (7) (2005) 2049–2057.

[13] L. A. Barrales Mora, V. Mohles, L. S. Shvindlerman, G. Gottstein, Effect of a finite quadruple junction mobility on grain microstructure evolution: Theory and simulation, Acta Materialia 56 (5) (2008) 1151–1164.

[14] B. Zhao, G. Gottstein, L. S. Shvindlerman, Triple junction effects in solids, Acta Materialia 59 (9) (2011) 3510–3518.

[15] C. E. Krill, L. Helfen, D. Michels, H. Natter, A. Fitch, O. Masson, R. Birringer, Size-dependent grain-growth kinetics observed in nanocrystalline fe, Physical Review Letters 86 (5) (2001) 842–845.

[16] H. Paul, C. E. Krill Iii, Anomalously linear grain growth in nanocrystalline fe, Scripta Materialia 65 (1) (2011) 5–8.

[17] L. A. Barrales-Mora, G. Gottstein, L. S. Shvindlerman, Effect of a finite boundary junction mobility on the growth rate of grains in two-dimensional polycrystals, Acta Materialia 60 (2) (2012) 546–555.

[18] D. Zöllner, A potts model for junction limited grain growth, Computational Materials Science 50 (9) (2011) 2712–2719.

[19] D. Zöllner, Grain microstructure evolution in two-dimensional polycrystals under limited junction mobility, Scripta Materialia 67 (1) (2012) 41–44.

[20] D. Weygand, Y. Bréchet, J. Lépinoux, A vertex dynamics simulation of grain growth in two dimensions, Philosophical Magazine Part B 78 (4) (1998) 329–352.

[21] D. Weygand, Y. Bréchet, J. Lépinoux, Influence of a reduced mobility of triple points on grain growth in two dimensions, Acta Materialia 46 (18) (1998) 6559–6564.

[22] R. Darvishi Kamachali, I. Steinbach, 3-d phase-field simulation of grain growth: Topological analysis versus mean-field approximations, Acta Materialia 60 (67) (2012) 2719–2728.

[23] R. Darvishi Kamachali, A. Abbondandolo, K. F. Siburg, I. Steinbach, Geometrical grounds of mean field solutions for normal grain growth, Acta Materialia 90 (0) (2015) 252–258.

[24] K. Kawasaki, T. Nagai, K. Nakashima, Vertex models for two-dimensional grain growth, Philosophical Magazine Part B 60 (3) (1989) 399–421.

[25] L. A. Barrales-Mora, L. S. Shvindlerman, V. Mohles, G. Gottstein, The effect of grain boundary junctions on grain microstructure evolution: 3D vertex simulation, Materials Science Forum 558-559 (2007) 1051–1056.

[26] L. A. Barrales-Mora, 2D and 3D grain growth modeling and simulation, Cuvillier Verlag, 2008.

[27] L. A. Barrales Mora, 2D vertex modeling for the simulation of grain growth and related phenomena, Mathematics and Computers in Simulation 80 (7) (2010) 1411–1427.

[28] L.-Q. Chen, Phase-field models for microstructure evolution, Annual Review of Materials Research 32 (1) (2002) 113–140.

[29] I. Steinbach, F. Pezzolla, B. Nestler, M. Seeelberg, R. Prieler, G. J. Schmitz, J. L. L. Rezende, A phase field concept for multiphase systems, Physica D: Nonlinear Phenomena 94 (3) (1996) 135–147.

[30] A. Kazaryan, Y. Wang, S. A. Dregia, B. R. Patton, Grain growth in anisotropic systems: comparison of effects of energy and mobility, Acta Materialia 50 (10) (2002) 2491–2502.

[31] A. Kazaryan, B. R. Patton, S. A. Dregia, Y. Wang, On the theory of grain growth in systems with anisotropic boundary mobility, Acta Materialia 50 (3) (2002) 499–510.

[32] D. Zöllner, P. Streitenberger, Three-dimensional normal grain growth: Monte carlo potts model simulation and analytical mean field theory, Scripta Materialia 54 (9) (2006) 1697–1702.

[33] C. Mießen, N. Velinov, L. Barrales-Mora, G. Gottstein, to be published.

[34] J. Taylor, J. Cahn, Linking anisotropic sharp and diffuse surface motion laws via gradient flows, Journal of Statistical Physics 77 (1-2) (1994) 183–197.

[35] L. Evans, Partial Differential Equations, American Mathematical Society, 1998.

[36] C. H. Rycroft, Voro++: A three-dimensional voronoi cell library in c++, Chaos: An Interdisciplinary Journal of Nonlinear Science 19 (4) (2009) 041111.

[37] U. Czubayko, V. G. Sursaeva, G. Gottstein, L. S. Shvindlerman, Influence of triple junctions on grain boundary motion, Acta Materialia 46 (16) (1998) 5863–5871.

[38] S. G. Protasova, G. Gottstein, D. A. Molodov, V. G. Sursaeva, L. S. Shvindlerman, Triple junction motion in aluminum tricrystals, Acta Materialia 49 (13) (2001) 2519–2525.

[39] O. Nemitz, Anisotrope Verfahren in der Bildverarbeitung: Gradientenflüsse, Level-Sets und Narrow Bands, Dissertation, Universität Bonn, http://numod.ins.uni-bonn.de/research/papers/public/Ne08.pdf (2008).

[40] D. A. Rajon, W. E. Bolch, Marching cube algorithm: review and trilinear interpolation adaptation for image-based dosimetric models, Computerized Medical Imaging and Graphics 27 (5) (2003) 411–435.

[41] W. W. Mullins, Two dimensional motion of idealized grain boundaries, Journal of Applied Physics 27 (8) (1956) 900–904.